

Phases dynamics in VCSELs with delayed optical feedback and cross re-injection

J. Javaloyes⁽¹⁾, M. Marconi⁽²⁾ and M. Giudici⁽²⁾

⁽¹⁾ *Departament de Física, Universitat de les Illes Balears, C/ Valldemossa km 7.5, 07122 Mallorca, Spain*

⁽²⁾ *Institut Non-Linéaire de Nice, Université de Nice Sophia Antipolis, CNRS UMR 7335, 06560 Valbonne, France*

We study theoretically the non linear polarization dynamics of Vertical-Cavity Surface-Emitting Lasers in the presence of an external cavity providing delayed optical feedback and cross polarization re-injection. We show that far from the laser threshold, the dynamics remains confined close to the equatorial plane of a Stokes sphere of a given radius and we reduce the dynamics to a dynamical system composed of two phases: the orientation phase of the quasi-linear polarization and the optical phase of the field. We explore the complex modal structure given by the double feedback configuration and recovers as particular cases the Lang-Kobayashi modes and the modes found by Giudici et al. [1]. We also re-interpret the square waves switching dynamics as phase kinks.

I. INTRODUCTION

Vertical-cavity surface-emitting lasers (VCSELs) possess several advantages compared to conventional semiconductor edge-emitting lasers. Their circular aperture induces a high beam quality as compared to the strongly astigmatic output of edge emitters. In addition, the possibility to couple them efficiently to optical fiber as well as the possibility to perform on-wafer testing renders them superior to classical laser diodes.

VCSELs of large transverse dimensions can present rich spatio-temporal transverse dynamics [2–4], which can be harnessed for instance in order to create transverse localized structures[5, 6]. However, such complexity can be avoided by choosing a VCSEL only a few micrometers wide thereby limiting the number of transversal modes and since VCSELs are also intrinsically single-longitudinal mode, one may consider them ideal single mode devices.

However, these devices exhibit a nearly degenerate polarization orientation owing to their almost perfect symmetry around the cavity axis. Usually, the two polarization modes are aligned along the $[1\ 1\ 0]$ and the $[1\ -1\ 0]$ crystallographic axes, although some randomness exists due to the presence of hardly controllable strain [7]. In addition to the complex problem of the elasto-optic effects [8], the application of a voltage to the laser diode can also induce anisotropies via an electro-optic effect [9]. The existence of such favored directions is sufficient to weakly pin the polarization orientation dynamics and to define two optical modes having slightly different losses and frequencies. Such residual anisotropies are termed dichroism and birefringence in the cavity.

These two modes exhibit a high degree of coupling as they share an identical transverse spatial profile and the same carrier reservoir allowing for the existence of complex polarization dynamics. VCSELs are prone to display polarization switching [10–12] accompanied in some cases by regions of polarization bistability or even regimes where the polarization of the output oscillate in time [13].

In addition, the quasi-degeneracy of the orthogonal polarization states in VCSELs enables efficient cross-gain modulation among orthogonal polarizations when the de-

vice is used as an optical amplifier. In particular, VCSELs have been proposed as promising devices for implementing useful dynamics taking advantage of their polarization degree of freedom [14]. When VCSELs are subject to optical feedback, the polarization stability is affected and polarization dynamics appear even in the case of perfectly isotropic feedback [15]. Polarization-rotated optical feedback—where the two linearly polarized components, LP-x and LP-y, of the light emitted by the device are fed back into the laser cavity after the LP-x component is converted into the LP-y component and vice-versa—induces a regular polarization dynamics which can be as fast as 9 GHz [16, 17]. Such symmetrical cross re-injection was found to induce waveforms ranging from square-waves to sinusoidal oscillations.

Asymmetrical cross polarization re-injection (XPR), of a single polarization into the orthogonal one, was also shown to promote the occurrence of square wave switching [1] between orthogonal polarization with a repetition period close to twice the delay taken by the light to come back into the rotated orientation. The quasi-degeneracy of the VCSEL allows finding rather easily this regime which also exists in edge-emitting devices [18] yet for higher threshold of XPR. The analysis of laser system with multiple delays and different type of optical feedback are however not widespread. A few years ago some of the authors have proposed to combine XPR with polarization selective optical feedback (PSF), in order to achieve passive mode-locking in VCSELs [19, 20]. Recently, we also showed that PSF can be used to tune and control the existence of the square wave switching generated by XPR [?]. However, VCSELs must be described by a relatively high dimensional dynamical system that would consider the dynamics of the two polarizations as well as their interplay for the two carriers reservoirs with opposite spin orientations. This fact, in addition to the presence of two different time delays, render the analysis formidable a problem and a reduction to a lower dimensional system as presented in [21] for a solitary VCSEL close to the laser threshold, would be highly beneficial.

In this manuscript we show that far from the laser threshold, the dynamics of the VCSEL remains confined close to the equatorial plane of a Stokes sphere of a given

radius. This allows us to decouple the relaxation oscillation for the total emitted power as well as the fluctuations in the ellipticity of the emitted light. We reduce the dynamics to a dynamical system composed of two phases: the orientation phase of the quasi-linear polarization and the optical phase of the field.

We believe that such phase model and the general methodology employed here can be useful to harness the phase and orientation dynamics of VCSEL far from threshold, an important parameter regime for most applications. Indeed, such reduction not only allows to simplify the analytical and numerical studies but it may also be useful to get insight into future applications. While optical information is usually encoded in binary levels of light intensity, next generation communication systems will process not only intensity but also phase and the polarization data. Here, the simplicity of the phase model allowed us to explore the complex modal structure given by the double feedback configuration but also to re-interpret the square waves switching dynamics [19, 20, 22] as polarization orientation kinks.

The manuscript is organized as follows. In section II we briefly recall the basis of the model we use and fix the order of magnitude of the parameters for which our analysis applies. Section III is devoted to the phase reduction while we discuss the modal structure of our model in section IV. Perspective and conclusions are drawn in section V.

II. THE MODEL

We base our theoretical analysis on the so-called spin-flip model (SFM) [23], suitably modified for incorporating the effects of PSF and XPR. We assume that the LP-y mode is feedback into itself (PSF) and cross re-injected into the LP-x mode (XPR). While the most direct way to incorporate XPR and PSF would be in terms of the linearly polarized components of the field, X and

Y , the derivation of the phase model is more natural in the circular basis. The SFM model expressed in circular component reads

$$\dot{E}_{\pm} = (1 + i\alpha) (G_{\pm} - 1) E_{\pm} - zE_{\mp} + C_{\pm}, \quad (1)$$

$$T\dot{D}_{\pm} = 1 + P - D_{\pm} - G_{\pm} |E_{\pm}|^2 \mp \gamma_J (D_+ - D_-), \quad (2)$$

where E_{\pm} are the amplitudes of the circular left and right components of the field and D_{\pm} are the scaled carrier density in the two spin channels. In the equations (1-2), time has been scaled to the cavity decay rate κ , while $T = \kappa/\gamma_e$ represents the scaled carrier lifetime and γ_s is the spin-flip and carrier relaxation rate normalized to γ_e . The rate of carrier density injected into the active region above threshold is represented by P . In addition, α stands for the linewidth enhancement factor [24] and the complex parameter $z = \gamma_a + i\gamma_p$ is composed of the linear dichroism γ_a and the birefringence γ_p . We introduced the effect of ultra-fast gain saturation in the expression of the gain as

$$G_{\pm} = D_{\pm} \left(1 - \frac{\varepsilon_g}{2} |E_{\pm}|^2\right) \quad (3)$$

with the parameter of self-saturation ε_g . Since each component of the field only interacts with only one of the two spin channels, direct cross saturation between E_+ and E_- does not exist. Several sources can contribute to the factor ε_g like for instance spatial hole burning, spectral hole burning as well as carrier heating. In the case where the Y component is being feedback with complex rate $\eta \exp(-i\Omega)$ after a time τ_f and cross re-injected into the X polarization with a rate $\beta \exp(-ia)$, the expression of C_{\pm} reads

$$C_{\pm} = \frac{\beta}{2i} e^{-ia} (E_+^{\tau_r} - E_-^{\tau_r}) \pm \frac{\eta}{2} e^{-i\Omega} (E_+^{\tau_f} - E_-^{\tau_f}). \quad (4)$$

The modulus M_{\pm} and phase F_{\pm} decomposition of C_{\pm} as defined as $C_{\pm} = M_{\pm} \exp(iF_{\pm})$ is

$$\begin{aligned} M_+ &= \frac{\beta}{2} R_+^{\tau_r} \sin(\psi_+^{\tau_r} - \psi_+ - a) - \frac{\beta}{2} R_-^{\tau_r} \sin(\psi_-^{\tau_r} - \psi_+ - a) + \frac{\eta}{2} R_+^{\tau_f} \cos(\psi_+^{\tau_f} - \psi_+ - \Omega) - \frac{\eta}{2} R_-^{\tau_f} \cos(\psi_-^{\tau_f} - \psi_+ - \Omega) \\ M_- &= \frac{\beta}{2} R_+^{\tau_r} \sin(\psi_+^{\tau_r} - \psi_- - a) - \frac{\beta}{2} R_-^{\tau_r} \sin(\psi_-^{\tau_r} - \psi_- - a) - \frac{\eta}{2} R_+^{\tau_f} \cos(\psi_+^{\tau_f} - \psi_- - \Omega) + \frac{\eta}{2} R_-^{\tau_f} \cos(\psi_-^{\tau_f} - \psi_- - \Omega), \\ F_+ &= -\frac{\beta}{2} R_+^{\tau_r} \cos(\psi_+^{\tau_r} - \psi_+ - a) + \frac{\beta}{2} R_-^{\tau_r} \cos(\psi_-^{\tau_r} - \psi_+ - a) + \frac{\eta}{2} R_+^{\tau_f} \sin(\psi_+^{\tau_f} - \psi_+ - \Omega) - \frac{\eta}{2} R_-^{\tau_f} \sin(\psi_-^{\tau_f} - \psi_+ - \Omega), \\ F_- &= -\frac{\beta}{2} R_+^{\tau_r} \cos(\psi_+^{\tau_r} - \psi_- - a) + \frac{\beta}{2} R_-^{\tau_r} \cos(\psi_-^{\tau_r} - \psi_- - a) - \frac{\eta}{2} R_+^{\tau_f} \sin(\psi_+^{\tau_f} - \psi_- - \Omega) + \frac{\eta}{2} R_-^{\tau_f} \sin(\psi_-^{\tau_f} - \psi_- - \Omega). \end{aligned} \quad (5)$$

A. Parameters range

The polarization switchings in the SFM have been exhaustively analyzed in the literature [21, 25]; Here,

we consider the case where the VCSEL may displays a large ranges of bistability close to threshold and as such we consider small dichroism and birefringence typically of the order of a few GHz. Typically, we take

$\gamma_p = +5.24 \times 10^{-2}$, which means that we denote by LP-x the reddest mode and $\gamma_a = 0$. Besides, we assume standard values for the Henry's factor, $\alpha = 2$, a normalized carrier lifetime $T = 500$, and a typical normalized spin-flip rate $\gamma_s = 75$. The other typical values of the parameters are $\eta \sim 0.05$, $\beta \sim 0.05$, $\varepsilon_g = 0.02$ and $P = 10$ while the variance of the Gaussian white noise is 2×10^{-2} .

The presence of two kinds of feedback with possibly dissimilar delays render the analysis of Eqs. (1-2) formidable a problem. However, far from threshold one expects the dynamics that involves the relaxations oscillations between the total emitted power and the carrier reservoir to play only a minor role. Hence, in the following of this manuscript we will assume large bias current is $P \gtrsim 10$, which corresponds typically to relaxation oscillations of the order of $10 \sim 15$ GHz. In realistic situations the strong damping of the relaxations oscillations renders the laser almost a Class-A system, although such definition is meaningful only for a mono-mode system. Here, the standard “unsaturated” rate equations and the SFM do not reproduce fairly this regime of strong damping which explains why we included in our analysis the non linear saturation in Eq. (3). Noteworthy, a completely identical phase reduction as the one we discuss in this manuscript is possible without relying on gain saturation, yet for unrealistic parameter ranges, i.e. $P \sim 100$, corresponding to a device biased one hundred time above threshold. Several physical effects can contribute to the gain compression parameter ε_g like for instance spatial hole burning in the transverse plane of the VCSEL, spectral hole burning due to saturation of the individual intra-band transitions as well as carrier heating. The latter has the effect to spread the carriers within the band and to depopulate the available gain at the emission wavelength. In the following, we assumed that $\varepsilon_g \in \mathbb{R}$ which is consistent with a situation dominated by spatial hole burning, i.e. inter-band saturation.

III. PHASE REDUCTION

Far from threshold, the fluctuations of the total intensity will die out rapidly and the dynamics will be confined on a Stokes sphere of a given radius. Without external perturbation, one may not expect any complex residual dynamics since this center manifold is only two dimensional and consists in the polarization angle Φ and the ellipticity parameter θ , the optical phase being decoupled from the rest. In addition, strongly elliptical states would incur a large energetic penalty due to the imbalance between the two carrier reservoirs further confining the residual dynamics to the vicinity of the equatorial plane of the Stokes sphere and to polarization re-orientation.

Notwithstanding, the coherent delayed retro-actions imposed by the feedback terms in Eq. (4) the optical phase of the field couple back into the dynamics and as such our reduced model will consist in a “vectorial” phase

for the orientation of the quasi-linear polarization and for the optical phase of the field. It is worthwhile to notice that these two phases are of very different nature. While the optical phase precise value is irrelevant due to the phase invariance in an autonomous system the orientation phase is not because of the pinning imposed by the dichroism and the birefringence.

We now detail how the SFM with optical feedback and cross re-injection can be reduced to such phase model far from threshold. We start by separating the modulus and phase of the circular components by defining $E_{\pm} = R_{\pm} \sqrt{2} \exp(i\psi_{\pm})$, which yield with $\Phi = \psi_+ - \psi_-$

$$\begin{aligned} \dot{R}_+ &= (N + n - 1) R_+ - \gamma_a R_- \cos \Phi - \gamma_p R_- \sin \Phi \\ &\quad - \varepsilon_g (N + n) R_+^3 + M_+, \end{aligned} \quad (6)$$

$$\begin{aligned} \dot{R}_- &= (N - n - 1) R_- - \gamma_a R_+ \cos \Phi + \gamma_p R_+ \sin \Phi \\ &\quad - \varepsilon_g (N - n) R_-^3 + M_-, \end{aligned} \quad (8)$$

$$\begin{aligned} \dot{\psi}_+ &= \alpha (N + n - 1) + \gamma_a \frac{R_-}{R_+} \sin \Phi - \gamma_p \frac{R_-}{R_+} \cos \Phi \\ &\quad - \alpha \varepsilon_g (N + n) R_+^2 + \frac{F_+}{R_+}, \end{aligned} \quad (9)$$

$$\begin{aligned} \dot{\psi}_- &= \alpha (N - n - 1) - \gamma_a \frac{R_+}{R_-} \sin \Phi - \gamma_p \frac{R_+}{R_-} \cos \Phi \\ &\quad - \alpha \varepsilon_g (N - n) R_-^2 + \frac{F_-}{R_-}, \end{aligned} \quad (10)$$

$$\begin{aligned} T \dot{N} &= 1 + P - N - (N + n) R_+^2 - (N - n) R_-^2 \\ &\quad + \varepsilon_g [(N + n) R_+^4 + (N - n) R_-^4], \end{aligned} \quad (11)$$

$$\begin{aligned} T \dot{n} &= -\gamma_s n - (N + n) R_+^2 + (N - n) R_-^2 \\ &\quad + \varepsilon_g [(N + n) R_+^4 - (N - n) R_-^4], \end{aligned} \quad (12)$$

where we defined the average carrier density an $N = (N_+ + N_-)/2$ and the imbalance between the two channels $n = (N_+ - N_-)/2$ as well as $\gamma_s = 1 + 2\gamma_j$. As previously mentioned, far from threshold we expect the dynamics of the field to be restricted to the vicinity of a Stokes sphere. We make that apparent by defining the radius $I = R_+^2 + R_-^2$ and the ratio of the two circular components which is a measure the degree of ellipticity $\theta = \arctan(R_-/R_+)$, hence $R_+ = \sqrt{I} \cos \theta$ and $R_- = \sqrt{I} \sin \theta$. We can relate the left (resp. right) circular components E_- (resp. E_+) in terms of the Stokes coordinates (S_0, S_1, S_2, S_3) as described in Fig. (1)

$$S_0 = |E_-|^2 + |E_+|^2 = 2I, \quad (13)$$

$$S_1 = 2\Re(E_-^* E_+) = 2I \sin(2\theta) \cos \Phi, \quad (14)$$

$$S_2 = -2\Im(E_-^* E_+) = 2I \sin(2\theta) \sin \Phi, \quad (15)$$

$$S_3 = |E_-|^2 - |E_+|^2 = 2I \cos(2\theta). \quad (16)$$

In addition we proceed to the scaling of Eqs. (6-12) to the natural time scale of the relaxation oscillation frequency ω_r as $s = \omega_r t$ and define

$$\omega_r = \sqrt{\frac{2P}{T}}, \quad D = \frac{2(N-1)}{\omega_r}, \quad d = \frac{2n}{\omega_r}, \quad \Gamma = \frac{\omega_r}{2} (1 + P^{-1}) \quad (17)$$

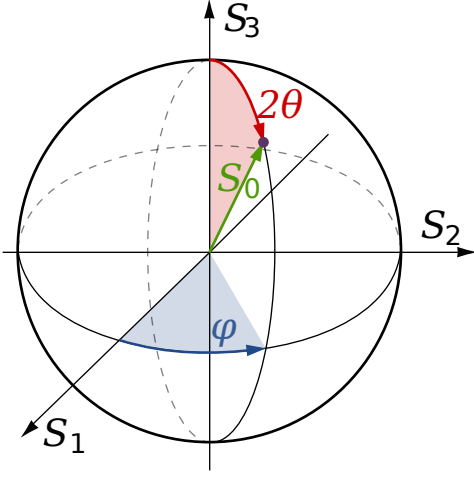


Figure 1: (Color Online): Angular representation of the VCSEL dynamics onto the Stokes sphere.

as well as the total intensity relatively to the steady value of the solitary laser $S = I/P$. With our typical values for the parameters far from threshold $P \sim 10$ and $\omega_r \sim 0.2$. As such $\Gamma \sim 0.1$ and the oscillations are only mildly damped, i.e. the laser performs ten oscillations before reaching its steady state in complete disagreement with any experimental evidence. Here, the presence of gain saturation strongly contributes to reduce the number of oscillation necessary to reach the equilibrium. Upon simplification of Eqs. (6-12) we get

$$\frac{dS}{ds} = DS + dS \cos(2\theta) - 2\frac{\gamma_a}{\omega_r} S \sin(2\theta) \cos \Phi - 2\frac{\varepsilon_g P}{\omega_r} S^2 \mathcal{A}(S, \theta) + \frac{\mathcal{F}(S, \theta)}{\omega_r} \quad (18)$$

$$\frac{d\theta}{ds} = -\frac{d}{2} \sin(2\theta) - \frac{\gamma_a}{\omega_r} \cos(2\theta) \cos \Phi + \frac{\gamma_p}{\omega_r} \sin \Phi + \frac{\varepsilon_g P}{4\omega_r} S \mathcal{B}(S, \theta) + \frac{\mathcal{G}(S, \theta)}{\omega_r} \quad (19)$$

$$\frac{d\psi_+}{ds} = \frac{\alpha}{2} (D + d) + \frac{\gamma_a}{\omega_r} \tan \theta \sin \Phi - \frac{\gamma_p}{\omega_r} \tan \theta \cos \Phi - \alpha \frac{\varepsilon_g P}{\omega_r} \mathcal{H}_+(S, \theta) + \frac{F_+}{\omega_r R_+} \quad (20)$$

$$\frac{d\psi_-}{ds} = \frac{\alpha}{2} (D - d) - \frac{\gamma_a}{\omega_r} \cotan \theta \sin \Phi - \frac{\gamma_p}{\omega_r} \cotan \theta \cos \Phi - \alpha \frac{\varepsilon_g P}{\omega_r} \mathcal{H}_-(S, \theta) + \frac{F_-}{\omega_r R_-} \quad (21)$$

$$\frac{dD}{ds} = -\Gamma D - \left(1 + \frac{\omega_r D}{2}\right) (S - 1) \quad (22)$$

$$- \frac{\omega_r dS}{2} \cos(2\theta) + \frac{\varepsilon_g P}{2} S^2 + \dots \quad (23)$$

$$\frac{dd}{ds} = -\frac{\omega_r}{2} d \left(\frac{\gamma_s}{P} + S \right) - \left(1 + \frac{\omega_r}{2} D\right) S \cos(2\theta), \quad (24)$$

In the equations (18-21), we separated on the first and

second lines the natural contributions of the SFM model from the ones due to feedbacks and non linear gain compression. The definitions of $\mathcal{A}, \mathcal{B}, \mathcal{H}_\pm, \mathcal{F}$ and \mathcal{G} are

$$\mathcal{A}(S, \theta) = \left[1 + \frac{\omega_r}{2} (D + d)\right] \cos^4 \theta + \left[1 + \frac{\omega_r}{2} (D - d)\right] \sin^4 \theta \quad (25)$$

$$\mathcal{B}(S, \theta) = \left(1 + \frac{\omega_r}{2} D\right) \sin(4\theta) + \omega_r d \sin(2\theta) \quad (26)$$

$$\mathcal{H}_+(S, \theta) = \left(1 + \frac{\omega_r}{2} (D + d)\right) S \cos^2 \theta \quad (27)$$

$$\mathcal{H}_-(S, \theta) = \left(1 + \frac{\omega_r}{2} (D - d)\right) S \sin^2 \theta \quad (28)$$

$$\mathcal{F}(S) = 2 \frac{R_+ M_+ + R_- M_-}{P} \quad (29)$$

$$\mathcal{G}(S) = \frac{M_- R_+ - M_+ R_-}{SP} \quad (30)$$

In addition, we neglected several terms in the carrier equations Eq. (22) and Eq. (24) which are due to non linear saturation. These terms are of order $\mathcal{O}(\varepsilon_g P \omega_r)$ and are immaterial to our analysis. The dominant effect of gain compression is to create an additional damping in the field equation leaving the carrier dynamics essentially unchanged up to second order.

The equations (18-24) can be further simplified if one assume the following scaling of the parameters. We define $\varepsilon \sim 0.2$ as our smallness parameter such that $\omega_r \sim \varepsilon$ and we consider the case where η and β as well as γ_a and γ_p are of order ε^2 . Importantly, we assume that the gain compression coefficient ε_g is also of order ε^2 although since $P \sim 10$, the contribution $\varepsilon_g \omega_r^{-1} P$ is considered to be of order one. At last we assume that the spin-flip decay term scales like $\gamma_s \sim \varepsilon^{-2}$.

We expand the flow around a solution defined by a quasi-linear, yet undefined polarization. In other terms we assume that there is little ellipticity, i.e. $\theta_0 \sim \pi/4$ and $d_0 = 0$. Besides, we assume that the radius of the Stokes sphere is close to its steady state value $S \sim S_0$ and consequently the carriers are also around their equilibrium value $D = D_0$. In order to make apparent the scale separation between the orientation of the polarization angle and the rest of the variables, we introduce two time scales as

$$\frac{d}{ds} = \frac{\partial}{\partial \sigma_0} + \varepsilon \frac{\partial}{\partial \sigma_1} \quad (31)$$

as well as the following series expansion

$$\begin{aligned} S &= S_0 + \varepsilon S_1(\sigma_0, \varepsilon \sigma_1) + \mathcal{O}(\varepsilon^2) \\ \theta &= \theta_0 + \varepsilon \theta_1(\sigma_0, \varepsilon \sigma_1) + \mathcal{O}(\varepsilon^2) \\ D &= D_0 + \varepsilon D_1(\sigma_0, \varepsilon \sigma_1) + \mathcal{O}(\varepsilon^2) \\ d &= d_0 + \varepsilon d_1(\sigma_0, \varepsilon \sigma_1) + \mathcal{O}(\varepsilon^2) \end{aligned} \quad (32)$$

while $\psi_\pm(\sigma_0, \varepsilon \sigma_1)$ is not expanded perturbatively. As such, the orientation $\Phi = \psi_+ - \psi_-$ can evolve freely between 0 and 2π . At the zeroth order, we get the following

system

$$\frac{\partial S_0}{\partial \sigma_0} = D_0 S_0 - \frac{\varepsilon_g P}{\omega_r} S_0^2, \quad , \quad \frac{\partial D_0}{\partial \sigma_0} = 1 - S_0, \quad (33)$$

where we notice that with our scaling of parameters the relaxation oscillations would not be damped if it wasn't for the non linear gain saturation contribution. We find that $S_0 = 1$ and $D_0 = \varepsilon_g P \omega_r^{-1}$. Nicely the phases ψ_{\pm} do not depend on the fast time scale since the two zeroth order contributions cancel each other, i.e.

$$\frac{\partial \psi_{\pm}}{\partial \sigma_0} = 0 \quad (34)$$

The first order problem reads on the fast time scale σ_0

$$\frac{\partial S_1}{\partial \sigma_0} = -D_0 S_1 + D_1 - 2 \frac{\gamma_a}{\omega_r} \cos \Phi - \frac{\varepsilon_g P}{2} D_0 + \frac{\mathcal{F}_0}{\omega_r}, \quad (35)$$

$$\frac{\partial \theta_1}{\partial \sigma_0} = -\frac{d_1}{2} - \frac{\gamma_a}{\omega_r} \cos \Phi + \frac{\gamma_p}{\omega_r} \sin \Phi - \frac{\varepsilon_g P}{\omega_r} \theta_1 + \frac{\mathcal{G}_0}{\omega_r} \quad (36)$$

$$\frac{\partial D_1}{\partial \sigma_0} = -\Gamma D_0 - S_1 + \frac{\varepsilon_g P}{2}, \quad (37)$$

$$\frac{\partial d_1}{\partial \sigma_0} = -\frac{\omega_r}{2} \frac{\gamma_s}{P} d_1 + 2\theta_1. \quad (38)$$

We notice that Eqs. (35,37) and Eqs. (36,38) correspond to two decoupled damped oscillators. While ellipticity oscillations between (d_1, θ_1) in Eqs. (36,38) are strongly damped with a rate $\omega_r \gamma_s P^{-1}$, the total intensity

and carrier oscillations in Eqs. (35,37) need the damping due to the non linear saturation. This effect is actually hidden in the fact that $D_0 \neq 0$. These two oscillators are forced by the feedback terms \mathcal{F}_0 and \mathcal{G}_0 , the latter being evaluated at zeroth order since they are proportional to η and β and therefore already first order quantities. At this order in the expansion, these terms depend only the slow time scale σ_1 through their dependence on variables ψ_{\pm} . We can therefore readily solve Eqs. (35-37) at steady state and inject the adiabatic result in the first order problem for ψ_{\pm} on the slow time σ_1 that reads

$$\begin{aligned} \frac{d\psi_+}{d\sigma_0} &= \frac{\alpha}{2} (D_1 + d_1) + \gamma_a \tan \theta \sin \Phi - \gamma_p \tan \theta \cos \Phi \\ &- \alpha \frac{\varepsilon_g P}{4} D_0 - \alpha \frac{D_0}{2} S_1 + \alpha \frac{\varepsilon_g P}{\omega_r} \theta_1 + \frac{F_+^0}{\omega_r} \end{aligned} \quad (39)$$

$$\begin{aligned} \frac{d\psi_-}{d\sigma_0} &= \frac{\alpha}{2} (D_1 - d_1) - \gamma_a \cotan \theta \sin \Phi - \gamma_p \cotan \theta \cos \Phi \\ &- \alpha \frac{\varepsilon_g P}{4} D_0 - \alpha \frac{D_0}{2} S_1 - \alpha \frac{\varepsilon_g P}{\omega_r} \theta_1 + \frac{F_-^0}{\omega_r} \end{aligned} \quad (40)$$

Upon replacing D_1 and d_1 from the steady state expression of Eqs. (35,37), the several contributions due to non linear saturation ε_g cancel each other leaving only the dichroism, the birefringence and the feedback terms to drive the motion of ψ_{\pm} . After defining $u = \arctan(\alpha)$ and $\zeta = \arctan 2(\gamma_p, \gamma_a)$ we obtain the phase model for ψ_+ and ψ_- that reads, with $|z| = \sqrt{\gamma_a^2 + \gamma_p^2}$

$$\begin{aligned} \frac{1}{\sqrt{1+\alpha^2}} \frac{d\psi_{\pm}}{dt} &= |z| \sin(u \pm \psi_+ \mp \psi_- - \zeta) + \frac{\beta}{2} [-\cos(\psi_+^{\tau_r} - \psi_{\pm} - a - u) + \cos(\psi_-^{\tau_r} - \psi_{\pm} - a - u)] \\ &\pm \frac{\eta}{2} [\sin(\psi_+^{\tau_f} - \psi_{\pm} - \Omega - u) - \sin(\psi_-^{\tau_f} - \psi_{\pm} - \Omega - u)] \end{aligned} \quad (41)$$

where we reintroduced the original time scale in Eq. (41) to clarify that the characteristic time scale is governed by the amplitude of the terms γ_a, γ_p, η and β . Notice however that the dynamics may not be restricted to a particularly slow time scales as the main requirement for our analysis to hold is for the four aforementioned parameters to be smaller than the damping of the relaxation oscillations which is typically $10 \sim 15$ GHz, hence studying multi-GHz dynamics would still be possible within our simplified approach. At last, we stress that it is not because we reduced the dynamics to the evolution of the equatorial component on the Stokes Sphere Φ that the dynamics is confined to purely linear polarization. Indeed, we can express θ and n solving Eqs. (36,38) as

$$\theta(\psi_+ - \psi_-) = \frac{\pi}{4} + \frac{\mathcal{G}_0 - |z| \cos(\zeta + \psi_+ - \psi_-)}{P(2\gamma_s^{-1} + \varepsilon_g)}, \quad (42)$$

and similarly for the spin imbalance $n = 2P(\theta - \frac{\pi}{4})\gamma_s^{-1}$.

Equivalent yet cumbersome expressions for the intensity and total carrier variations can be obtained in the same way. From Eq. (42), it is apparent that the typical deviations of θ with respect to $\pi/4$ and the spin-imbalance δn are

$$\delta\theta \sim \pm\pi/10, \quad n \sim \pm 0.1. \quad (43)$$

Notice that $\delta\theta = \pi/4$ would correspond to a purely circular emission state.

IV. RESULTS

The modal structure of the VCSEL submitted to optical feedback and cross-injection is more conveniently studied by defining the half sum $\Sigma = (\psi_+ + \psi_-)/2$ and the difference $\Phi = \psi_+ - \psi_-$. In the case of a mono-mode solution the difference Φ fixes the orientation of the quasi-

linear polarization and reaches a fix point while the half sum drifts at the frequency of the mode under consider-

ation. After some trigonometric simplifications Eq. (41) transforms into

$$\frac{1}{\sqrt{\cdot}} \frac{d\Sigma}{ds} = |z| \cos \Phi \sin(u - \zeta) - \eta \sin \frac{\Phi^{\tau_f}}{2} \sin \frac{\Phi}{2} \sin(u + \Omega + \Sigma - \Sigma^{\tau_f}) - \beta \cos \frac{\Phi}{2} \sin \frac{\Phi^{\tau_r}}{2} \sin(u + a + \Sigma - \Sigma^{\tau_r}), \quad (44)$$

$$\frac{1}{2\sqrt{\cdot}} \frac{d\Phi}{ds} = |z| \sin \Phi \cos(u - \zeta) + \eta \sin \frac{\Phi^{\tau_f}}{2} \cos \frac{\Phi}{2} \cos(u + \Omega + \Sigma - \Sigma^{\tau_f}) - \beta \sin \frac{\Phi}{2} \sin \frac{\Phi^{\tau_r}}{2} \cos(u + a + \Sigma - \Sigma^{\tau_r}) \quad (45)$$

with $\sqrt{\cdot} = \sqrt{1 + \alpha^2}$. Interestingly, the symmetry properties of Eqs. (44,45) are not equivalent with respect to Σ and Φ . While Eqs. (44,45) are phase invariant with respect to Σ , this is not the case for Φ . It is an expected result since these two phases do not have the same physical meaning, Σ is an optical phase while Φ is an orientation angle.

Mono-modes solutions correspond to $\Sigma = \omega t$ while Φ is a constant. Besides the value of ω and Φ we will represent the associated ellipticity θ using Eq. (42), exploiting that the expression of \mathcal{G}_0 in the case of a monochromatic solution simply read

$$\mathcal{G}_0 = 2\beta \sin^2 \frac{\Phi}{2} \sin(\omega\tau_r + a) - \eta \sin \Phi \sin(\omega\tau_f + \Omega) \quad (46)$$

A. Particular cases

Before studying the general case, we will recover several known situations as particular cases in the absence of any feedback or with only PSF.

Solitary VCSEL : We first discuss the stability of the solitary VCSEL that is governed by a single equation for Φ Eq. (45) that reads after simplification

$$\frac{d\Phi}{ds} = 2(\gamma_a + \alpha\gamma_p) \sin \Phi, \quad (47)$$

the solutions $\Phi_x = 0$ and $\Phi_y = \pi$ correspond respectively to a saddle and a node when $\gamma_a + \alpha\gamma_p > 0$, and vice-versa in the opposite case. The frequency of such two modes can be deduced from Eq. (44) that reads

$$\frac{d\Sigma}{ds} = (\alpha\gamma_a - \gamma_p) \cos \Phi_{x,y} = \omega_{x,y}. \quad (48)$$

The stability diagram is depicted in Fig. 2. Notice that the stability diagram of Fig. 2 is much simpler than for instance the analysis performed in [21]. For instance there is no bistability in our case like since we are far from threshold. However, we checked numerically the accuracy of the stability information predicted by Eq. 47 and found a good agreement, in the sense that the condition $\gamma_a + \alpha\gamma_p = 0$ indeeds separate mono-stable emission along LP-x from LP-y. However, even far from threshold, a very small region of bistability was found in the vicinity

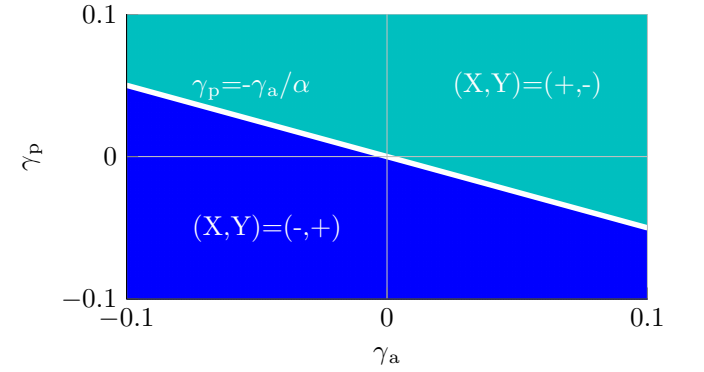


Figure 2: (Color Online): Stability diagram of the solitary VCSEL far from threshold. The condition $\gamma_a + \alpha\gamma_p = 0$ separates the two parameter regions where the stable emission is along the Y or the X axis. Stable (resp. instable) emission is depicted by a - sign (resp. a + sign).

of the line $\gamma_a + \alpha\gamma_p = 0$ represented in Fig. 2. Since our simplified model is build on a perturbative expansion, it is not abnormal that some small, usually negligible terms dominate the stability close to the special conditions in parameter space for which the first order term vanishes.

LP-x emission : Irrespectively of the values of η and β , pure emission along the X-axis of the solitary VCSEL is always possible since the existence of this mode is obviously not affected by optical feedback into Y and cross-injection of Y into X. This formally corresponds to the solution $\Phi = 0$ which solves Eq. (45) while Eq. (44) reduces to the expression of the frequency of the X solution at frequency $-\gamma_p$ pulled by the interplay of the dichroism γ_a and α , i.e.

$$\omega_x = \sqrt{1 + \alpha^2} |z| \sin(u - \zeta) = \alpha\gamma_a - \gamma_p \quad (49)$$

where we used trigonometrical identifies to simplify the last result.

LP-y Lang-Kobayashi modes : Secondly, on the case where there is only optical feedback, i.e. $\beta = 0$, the solution $\Phi = \pi$ solves Eq. (45). This case corresponds to a linear polarization along the Y axis and Eq. (44) reduces exactly to the locus of the modes of the Lang-

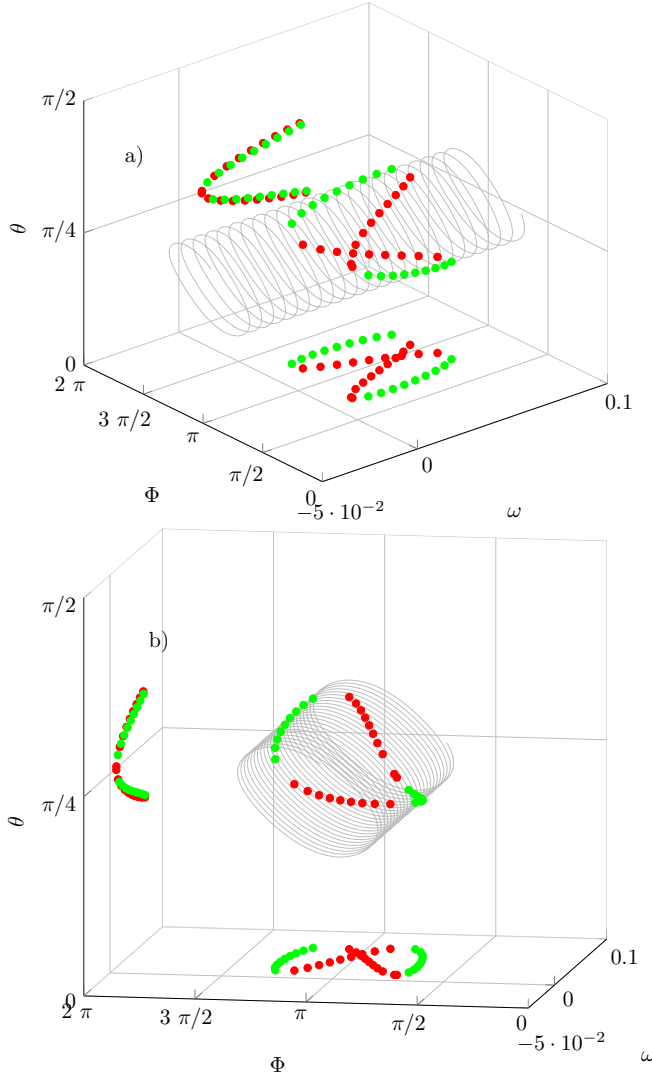


Figure 3: (Color Online): Monochromatic solutions of Eqs. (44,45) for $\eta = 0$, $\beta = 0.05$ and $\tau_r = 1000$. The solutions are arranged around a tube defined by the function $\Phi(\omega)$ and $\theta(\omega)$ assuming ω a continuous variable. Stable and unstable solutions are represented in green and red, respectively. The number of stable and unstable solutions (S, U) is (18, 19)

Kobayashi model

$$\omega_y - \gamma_p + \alpha\gamma_a + \eta\sqrt{1+\alpha^2}\sin(u + \Omega + \omega_y\tau_f) = 0 \quad (50)$$

at the only difference that the ellipse of the modes is shifted by the birefringence γ_p as well as the contribution $\alpha\gamma_a$.

In the general case, the presence of cross-polarization make it so that the orientation cannot perfectly align with the Y -axis, hence $\Phi \neq 0, \pi$. This allows simplifying Eq. (45) dividing by $\sin \Phi$ and to express the orientation as a function of the frequency as

$$\frac{\Phi}{2} = \arctan \frac{2|z|\cos(u - \zeta) + \eta\cos(u + \Omega + \omega\tau_f)}{\beta\cos(u + a + \omega\tau_r)} \quad (51)$$

Such value of Φ must be replaced in Eq. (44) to yield the locus of the quasi-linear modes as solutions of

$$\begin{aligned} \frac{\omega}{\sqrt{1+\alpha^2}} &= |z|\cos[\Phi(\omega)]\sin(u - \zeta) \\ &- \eta\sin^2\left[\frac{\Phi(\omega)}{2}\right]\sin(u + \Omega + \omega\tau_f) \\ &- \beta\sin[\Phi(\omega)]\sin(u + a + \omega\tau_r) \end{aligned} \quad (52)$$

B. Cross polarization only

In the case where the VCSEL is submitted to only cross-polarization re-injection, i.e. $\eta = 0$, we recover the results of [1] as a particular case. It was shown in [1] that modes appears as saddle-node bifurcations for increasing values of β , in addition to the pure Y solution of the solitary VCSEL that evolves due to the influence of β . It entails that there is usually $N/2 + 1$ modes and $N/2$ anti-modes. Notice however that in [1] the modal structure was found by solving exactly the Eqs. (1,2) and without exploiting the particular scaling of the parameters. As such the solution was found as a determinant of a complex system of equations. Here, one is able to recognizes by inspecting Eq. (52) that the locus for the modes is in essence very similar to the one of the Lang-Koyabashi model, i.e. a transcendental equation defining the frequencies.

In addition to the solution defined by the triplet (ω, Φ, θ) we represented $\Phi(\omega)$ and $\theta(\omega)$ as continuous functions of ω , the reason for doing so will be clarified in the next section. This corresponds to the black lines in Fig. 3. The information regarding the stability of the solutions was found using DdeBiftool [26] on the Eqs. (44,45). Importantly, one notices in Fig. 3 that purely linear emission corresponding to solutions for which with $\theta = \pi/4$ is possible. This demonstrates that cross polarization can have the effect to simply rotate the direction of emission. The modes “ellipse” is centered around the frequency $\omega_y = \gamma_p - \alpha\gamma_a$ of the pure Y emission state and the states closer to $\Phi = \pi$, i.e. whose polarization is close to the Y axis, are the one the most unstable. In Fig. 3, the external part of the projection in the (ω, Φ) plane (the stable modes in green) corresponds to the orientations farther from Y . Such modes can also present a small ellipticity. Notice that in Fig. 8 of [1], the variable n , or equivalently here θ , presented a height shaped curve. This was due to the larger values of $\beta = 0.25$ used in [1].

For increasing values of β more modes are created via saddle-node bifurcations and the ellipse grows, yet more and more of the stable modes at the exterior of the eight shaped projection becomes unstable up to the critical value $\beta^* = 2\sqrt{\gamma_a^2 + \gamma_p^2}$ where all the modes are unstable, see Fig. 3. This corresponds to the onset of square wave switching [1, 18] where the two orthogonal polarizations X and Y alternate a cycle of on-off emission in anti-phase

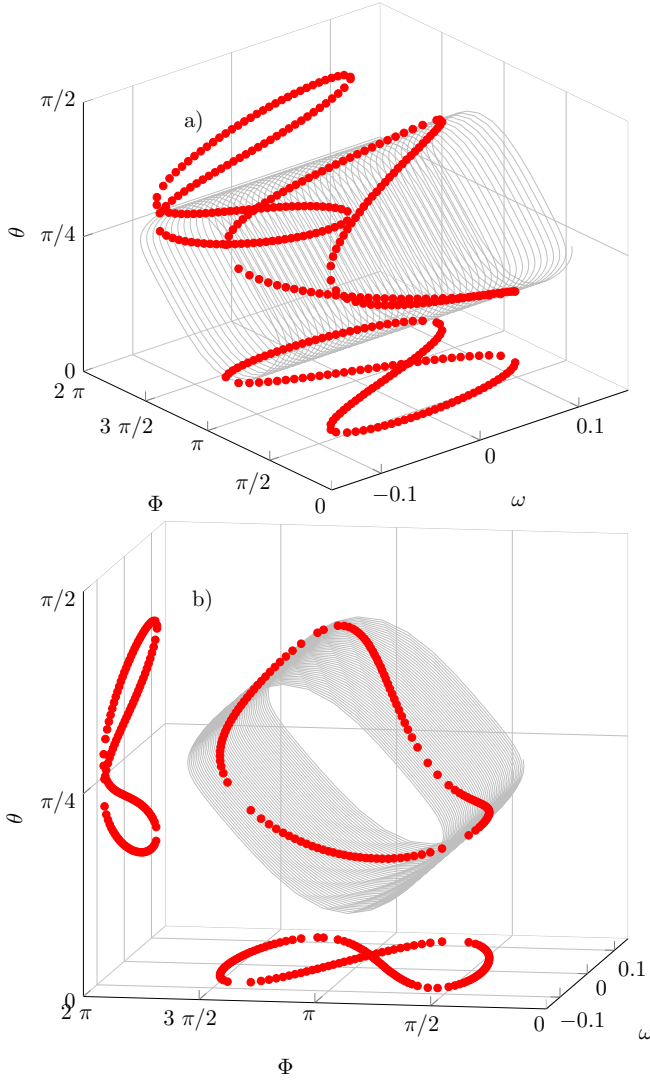


Figure 4: (Color Online): Monochromatic solutions of Eqs. (44,45) for $\eta = 0$, $\beta = \beta^* + 0.01$ and $\tau_r = 1000$. There are 127 unstable solutions. Stable and unstable solutions are represented in green and red, respectively.

and at a period close to twice the delay imposed by cross-polarization re-injection τ_r . Such dynamics at twice the delay is depicted in Fig. 5.

Here we reconstructed the intensity of the X and Y components via the formula $I_x \sim |1 + e^{i\Phi}|^2$ and $I_y \sim |1 - e^{i\Phi}|^2$. By construction, the anti-phase between the two polarization is perfect as one can notice in Fig. 5a). For $\beta > \beta^*$ we found in Fig. 5a) a strongly non linear limit cycle composed of two plateaus whose period is close to twice the re-injection delay τ_r in agreement with the results of [1, 18, 27]. Interestingly, we notice that it is possible to re-interpret such anti-phase dynamics for the intensities as a pure phase dynamics. Indeed we describe in Fig. 5b) the temporal evolution of Φ which consists in kinks between π and 0 and π again. The evolution of the global phase Σ consists mainly in a drift at a fre-

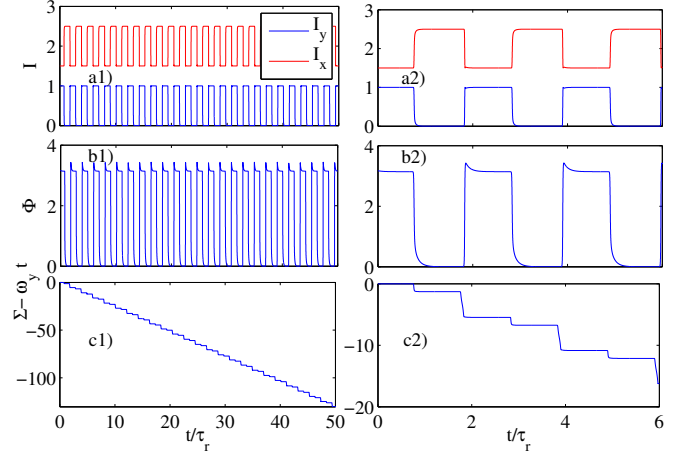


Figure 5: (Color Online): Square-wave switching as phase kinks. The panels a1) and a2) describe the intensity of the X and Y polarization over different time scales reconstructed from the polarization orientation Φ . The traces are shifted for clarity, and are actually in perfect anti-phase. The panels b1) and b2) represent the polarization orientation Φ while panels c1) and c2) describe the optical phase Σ to which we subtracted a drift $\omega_y t$. The parameters are $\eta = 0$, $\beta = \beta^* + 4 \times 10^{-3}$ and $\tau_r = 1000$.

quency ω_y , i.e. the frequency of the solitary VCSEL on the Y mode. This is consistent with the fact that the first plateau corresponds to pure Y emission while the second one consists in the Y mode performing injection locking into the X polarization. In both cases the frequency of emission is ω_y . Interestingly, once this drift is removed, a residual phase kink can be observed in Σ . However, such residual kinks in Σ are slaved to the square-wave switching and actually can be decoupled from the dynamics. For $\beta \gg \beta^*$ there is an excellent agreement between the full solution of Eqs. (44,45) and the one of Eq. (45) in which we performed the substitution $\Sigma - \Sigma_0 \rightarrow \omega_y \tau_r$ demonstrating that the square wave phenomena can be reduced to a single equation with delay of the type

$$\frac{d\Phi}{dt'} = \sin \frac{\Phi}{2} \left(\cos \frac{\Phi}{2} - A \sin \frac{\Phi_{\tau_r}}{2} \right) \quad (53)$$

where we scale time for clarity and defined an effective parameter

$$A = \frac{\beta \sqrt{1 + \alpha^2}}{2 \gamma_a + \alpha \gamma_p} \cos [u + a + (\gamma_p - \alpha \gamma_a) \tau_r] \quad (54)$$

Inspection of Eq. (53) reveals that solutions composed of plateaus of duration τ_r for which either $\Phi = 0$ or $\Phi = \pi$ are indeed possible.

C. Cross polarization and feedback

In the general case where both η and β are non zero, the modal structure depends critically on the difference

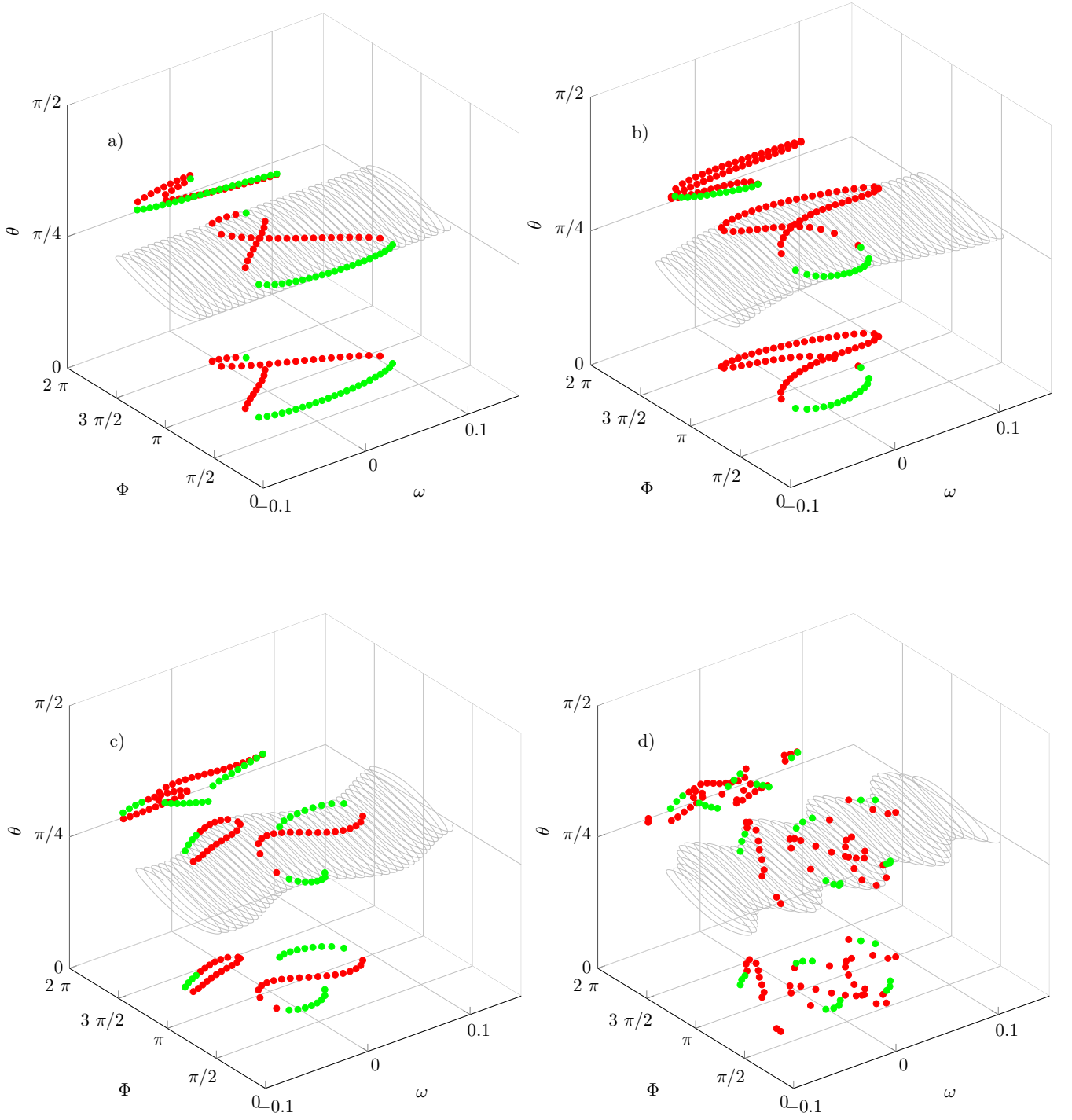


Figure 6: (Color Online): Monochromatic solutions of Eqs. (44,45) for $\eta = 0.025$, $\beta = 0.05$ and $\tau_r = 1000$. Panels a), b), c) and d) correspond to $\Delta\tau = \tau_f - \tau_r = 0$, $\Delta\tau = 20$, $\Delta\tau = 40$, and $\Delta\tau = 100$ for which the number of stable and unstable solutions (S, U) is $(24, 31)$, $(14, 55)$, $(21, 36)$ and $(15, 36)$

between the two delays. For small deviations for the situation $\tau_f = \tau_r$ the height shaped mode ellipse distorts and break in several parts as depicted in Fig. 6. Here, one notice that the tubular structure that supports the mode acquires a modulation that is proportional to the difference between the two delays. For small differences

between the two delays like in Fig. 6a) and Fig. 6b) the mode “ellipse” is deformed. For larger differences like e.g. in Fig. 5c) the modes position break into several sub families. Increasing the difference between the two delays beyond Fig. 6d) would give a modal structure that would seems like random points (not shown) if observed only

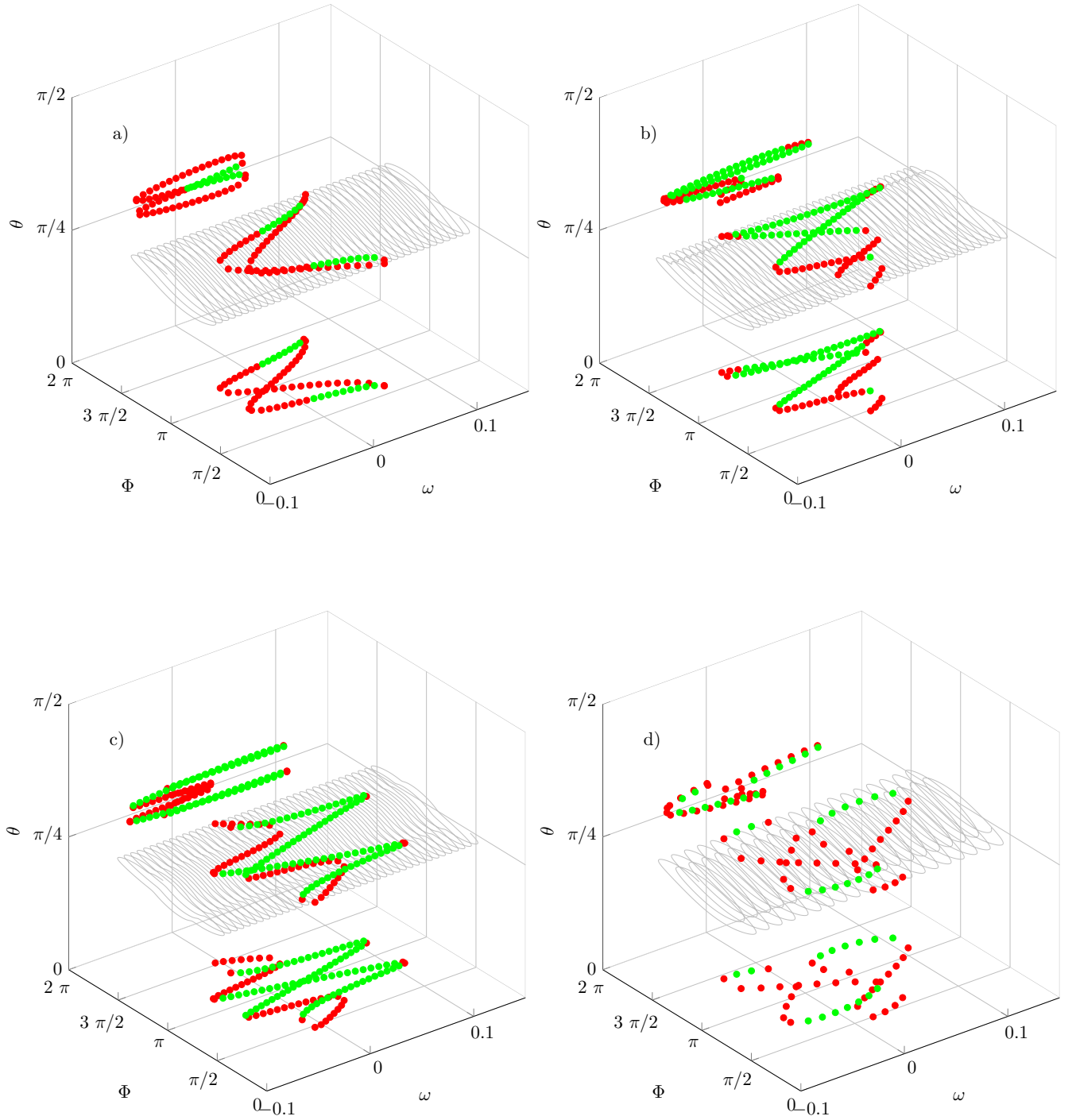


Figure 7: (Color Online): Monochromatic solutions of Eqs. (44,45) for $\eta = 0.025$, $\beta = 0.05$ and $\tau_r = 1000$. Panels a), b), c) and d) correspond to $\tau_f = 2\tau_r$, $\tau_f = 3\tau_r$, $\tau_f = 4\tau_r$, and $\tau_f = \tau_r/2$ for which the number of stable and unstable solutions (S, U) is $(17, 52)$, $(55, 36)$, $(82, 47)$ and $(15, 30)$

through a projection in the (ω, Φ) plane. We depicted in Fig. 6 a sequence for which τ_f is increased above τ_r , yet a similar scenario is found for $\tau_f < \tau_r$.

Once it is understood that the tubular structure oscillate at a frequency given by the difference between the two delays, one may foresee the existence of “revivals” of

relatively simple modal structures for specific ratio between the two delays. Indeed we show in Fig. 7 that a regular structure exists whenever the feedback delay is an integer of the cross polarization delay. Similarly, some simple structure were also found when $\tau_f = \tau_r/n$ and we depicted in Fig. 7d) the case $\tau_f = \tau_r/2$.

D. Influence of optical feedback onto the square wave switching

The second plateau of the square wave dynamics described in [1, 27] consists in the strong mode (say LP-y) injection locking the weak mode (say LP-x). At the end of the second plateau, the transitory dynamics can be understood as an escape of the vicinity of a possibly weakly repulsive saddle. During such escape the system is very sensible to noise which induces strong period jitter in the square wave signal. The non vanishing time needed to perform such an escape explains why the period of the square oscillation is always slightly superior to twice the XPR delay τ_r .

The proximity of bistable emission close to threshold and the existence of “dynamical traps” via the folding of some unstable limit cycles induced by XPR was already established in [1] as some likely mechanisms for the degradation of the square wave signal, see Fig.9 in [1] for instance. In our case, the system does not exhibit such bistability since we are far from threshold. Yet the proximity in parameter space of the line $\gamma_a + \alpha\gamma_p = 0$ depicted in Fig. 2 that interchange the stability of the X and Y solution can play a similar role. We describe in Fig. 8 such degraded square wave dynamics in the proximity of the parameter value $\gamma_a = -\alpha\gamma_p$ where the X and Y polarizations exchange their stability. Here also we integrated the phase model given by Eqs. (44,45) and reconstructed the intensity of the Y component as $I_y \sim |1 - e^{i\Phi}|^2$. In Fig. 8, the dynamics experiences a critical slowing down at the end of the second plateau where the LP-y component is off and the escape from the weak saddle can be imagined as a noise induced wandering in an almost flat landscape.

However, a small amount of optical feedback has the effect to re-stabilize the Y polarization and incidentally to accelerate the escape of the saddle represented by emission into the $\tilde{\text{NLP-x}}$ mode. We describe in Fig. 9 such regime and show that even in the proximity of polarization switching, robust square wave switching can be obtained for proper choice of the feedback delay, i.e. $\tau_r \sim 2\tau_r$.

V. CONCLUSIONS

In this manuscript we reduced the dynamics of the VCSEL far from the laser threshold to a model that consists in two phases: the orientation phase of the quasi-linear polarization and the optical phase of the field. We showed that the dynamics remains confined close to the equatorial plane of a Stokes sphere of a given radius which allowed us to decouple the relaxation oscillation for the total emitted power as well as the fluctuations in the ellipticity of the emitted light.

Such simplification allowed expressing analytically the modes in presence of XPR and PSF and to shed some light on the complex modal structure given by the double

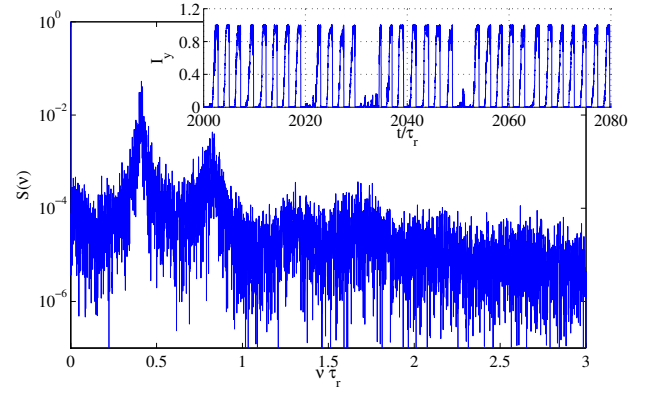


Figure 8: (Color Online): Square wave switching dynamics (inset) and power spectrum for $\eta = 0$, $\gamma_a = -0.09$, $\beta = 0.25$ and $\tau_r = 500$ and power spectrum. The signal is very irregular and the period is noticeably slower than $2\tau_r$. The power spectrum does not show the signature of a square wave signal with only odd harmonics.

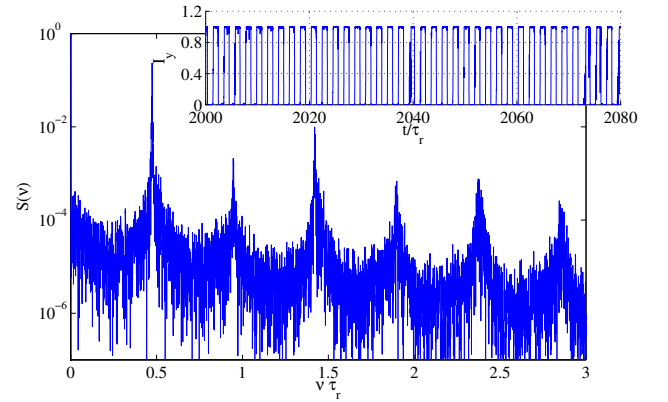


Figure 9: (Color Online): Square wave switching dynamics (inset) and power spectrum for $\eta = 0.05$, $\gamma_a = -0.09$, $\beta = 0.25$, $\tau_r = 500$ and $\tau_f = 1020$. The signal is much more regular, the period much closer than $2\tau_r$. The power spectrum shows the signature of a square wave signal with only odd harmonics.

feedback configuration. We also reinterpreted the square waves switching dynamics [19, 20, 22] previously found as polarization orientation kinks. Close to the polarization switching the stability of both the LP-y and LP-x modes becomes marginal which was shown to have a profound impact on the regularity of the anti-phase square wave switching induced by XPR. We showed that also in the reduced phase model the inclusion of optical feedback with a proper delay can have the effect to regularize the dynamics and that it can be used to mitigate the polarization degeneracy.

As future perspectives we believe that a similar approach can be applied to the case of isotropic rotated feedback. Such effect was shown to give anti-phase polarization oscillations [17] up to frequencies ~ 10 GHz. Our method would yield a similar phase model which would

allow studying such polarization dynamics possibly as a single dynamical equation. Also of great interest, our method can be extended readily to the case of polarized, and possibly detuned, optical injection.

Acknowledgments

We acknowledge fruitful discussions with Salvador Balle. J.J. acknowledges financial support from the Ramón y Cajal fellowship, the CNRS for supporting a

stay at the INLN where part of this work was developed as well as financial support from project RANGER (TEC2012-38864-C03-01) and from the Direcció General de Recerca, Desenvolupament Tecnològic i Innovació de la Conselleria d'Innovació, Interior i Justícia del Govern de les Illes Balears co-funded by the European Union FEDER funds. M.M. and M.G. acknowledge funding of Région "Provence-Alpes-Cote d'Azur" with the "Projet Volet Générale 2011 : Génération et Détection des Impulsions Ultra Rapides (GEDEPULSE)".

-
- [1] J. Mulet, M. Giudici, J. Javaloyes, and S. Balle. Square-wave switching by crossed-polarization gain modulation in vertical-cavity semiconductor lasers. *Phys. Rev. A*, 76:043801, Oct 2007.
 - [2] J. Mulet, S. Balle, M. San Miguel, and C. R. Mirasso. Transverse and polarization mode selection in vertical-cavity surface-emitting lasers. *IEEE 17th International Semiconductor Laser Conference*, pages 101–102, 2000.
 - [3] J. Mulet and S. Balle. Spatiotemporal optical model of VCSELs in the presence of polarization effects. *Quantum Electronics, IEEE Journal of*, 38:291–305, 2002.
 - [4] J. Mulet and S. Balle. Transverse mode dynamics in vcsels: Spatiotemporal versus modal expansion descriptions. *Physical Review A (Atomic, Molecular, and Optical Physics)*, 66:053802–8, 2002.
 - [5] S. Barland, J. R. Tredicce, M. Brambilla, L. A. Lugiato, S. Balle, M. Giudici, T. Maggipinto, L. Spinelli, G. Tissoni, T. Knodl, M. Miller, and R. Jager. Cavity solitons as pixels in semiconductor microcavities. *Nature*, 419(6908):699–702, Oct 2002.
 - [6] P. Genevet, S. Barland, M. Giudici, and J. R. Tredicce. Bistable and addressable localized vortices in semiconductor lasers. *Phys. Rev. Lett.*, 104:223902, Jun 2010.
 - [7] A. K. J. van Doorn, M. P. van Exter, and J. P. Woerdman. Elasto-optic anisotropy and polarization orientation of vertical-cavity surface-emitting semiconductor lasers. *Applied Physics Letters*, 69:1041–1043, 1996.
 - [8] G. Van der Sande, M. Peeters, I. Veretennicoff, J. Danckaert, G. Verschaffelt, and S. Balle. The effects of stress, temperature, and spin flips on polarization switching in vertical-cavity surface-emitting lasers. *Quantum Electronics, IEEE Journal of*, 42(9):898–906, sept. 2006.
 - [9] M. P. van Exter, A. K. J. van Doorn, and J. P. Woerdman. Electro-optic effect and birefringence in vertical-cavity surface-emitting lasers. *Physical Review A (Atomic, Molecular, and Optical Physics)*, 56:845–853, 1997.
 - [10] K. D. Choquette, D. A. Richie, and R. E. Leibenguth. Temperature dependence of gain-guided vertical-cavity surface emitting laser polarization. *Applied Physics Letters*, 64(16):2062–2064, 1994.
 - [11] S. Balle, E. Tolkachova, M. San Miguel, J. Tredicce, J. Martín-Regalado, and A. Gahl. Mechanisms of polarization switching in single-transverse-mode vertical-cavity surface-emitting lasers: thermal shift and nonlinear semiconductor dynamics. *xxx*, 24(16):1121–1123, 1999.
 - [12] T. Ackemann and M. Sondermann. Characteristics of polarization switching from the low to the high frequency mode in vertical-cavity surface-emitting lasers. *Applied Physics Letters*, 78(23):3574–3576, 2001.
 - [13] M. Sondermann, M. Weinkath, T. Ackemann, J. Mulet, and S. Balle. Two-frequency emission and polarization dynamics at lasing threshold in vertical-cavity surface-emitting lasers. *Phys. Rev. A*, 68:033822, Sep 2003.
 - [14] Krassimir Panajotov, Marc Sciamanna, Ignace Gatara, Mikel Arteaga, and Hugo Thienpont. Nonlinear dynamics of vertical-cavity surface-emitting lasers. *Advances in Optical Technologies*, 2011.
 - [15] M. Giudici, T. Ackemann, S. Barland, J. Tredicce, and S. Balle. Polarization dynamics in vertical-cavity surface-emitting lasers with optical feedback: experiment and model. *Journal of the Optical Society of America B*, 16(11):2114–2123, 1999.
 - [16] F. Robert, P. Besnard, M.L. Chares, and G.M. Stephan. Polarization modulation dynamics of vertical-cavity surface-emitting lasers with an extended cavity. *Quantum Electronics, IEEE Journal of*, 33(12):2231–2239, dec 1997.
 - [17] Hua Li, Angela Hohl, Athanasios Gavrielides, Hong Hou, and Kent D. Choquette. Stable polarization self-modulation in vertical-cavity surface-emitting lasers. *Applied Physics Letters*, 72(19):2355–2357, 1998.
 - [18] Athanasios Gavrielides, Thomas Erneux, David W. Sukow, Guinevere Burner, Taylor McLachlan, John Miller, and Jake Amonette. Square-wave self-modulation in diode lasers with polarization-rotated optical feedback. *Opt. Lett.*, 31(13):2006–2008, Jul 2006.
 - [19] Julien Javaloyes, Josep Mulet, and Salvador Balle. Passive mode locking of lasers by crossed-polarization gain modulation. *Phys. Rev. Lett.*, 97:163902, Oct 2006.
 - [20] J. Mulet, J. Javaloyes, and S. Balle. Mode-locking of vcsels by crossed-polarization gain modulation. *Quantum Electronics, IEEE Journal of*, 43(9):786–793, sept. 2007.
 - [21] T. Erneux, J. Danckaert, K. Panajotov, and I. Veretennicoff. Two-variable reduction of the San Miguel-Feng-Moloney model for vertical-cavity surface-emitting lasers. *Physical Review A (Atomic, Molecular, and Optical Physics)*, 59(6):4660–4667, 1999.
 - [22] David W. Sukow, Taylor Gilfillan, Brenton Pope, Maria S. Torre, Athanasios Gavrielides, and Cristina Masoller. Square-wave switching in vertical-cavity surface-emitting lasers with polarization-rotated optical feedback: Experiments and simulations. *Phys. Rev. A*,

- 86:033818, Sep 2012.
- [23] M. San Miguel, Q. Feng, and J. V. Moloney. Light-polarization dynamics in surface-emitting semiconductor lasers. *Physical Review A (Atomic, Molecular, and Optical Physics)*, 52(2):1728–1739, 1995.
 - [24] C. Henry. Theory of the linewidth of semiconductor lasers. *Quantum Electronics, IEEE Journal of*, 18(2):259–264, Feb 1982.
 - [25] J. Martín-Regalado, F. Prati, M. San Miguel, and N.B. Abraham. Polarization properties of vertical-cavity surface-emitting lasers. *Quantum Electronics, IEEE Journal of*, 33(5):765–783, 1997.
 - [26] Koen Engelborghs, Tatyana Luzyanina, and Giovanni Samaey. Dde-biftool v. 2.00: a matlab package for bifurcation analysis of delay differential equations. Technical report, Department of Computer Science, K.U.Leuven, Belgium., 2001.
 - [27] M. Marconi, J. Javaloyes, S. Barland, M. Giudici, and S. Balle. Robust square-wave polarization switching in vertical-cavity surface-emitting lasers. *Phys. Rev. A*, 87:013827, Jan 2013.